3

Geophysical Constraints on Hydrothermal Circulation

Observations and Models

A.T. FISHER

Earth Sciences Department, University of California,
Santa Cruz, CA 95064, U.S.A.

ABSTRACT

Geophysical observations and models provide important constraints on the properties of seafloor hydrothermal systems and associated fluxes. These studies indicate how the upper lithosphere is constructed and evolves, characteristics that are related to hydrothermal systems through the mechanical state of the lithosphere and the availability of heat to drive fluid flow. Geophysical studies illustrate correlations between the rate of seafloor spreading and the depth of an axial melt lens reflection, the occurrence and intensity of near-ridge seismicity, and advective heat output from hydrothermal systems. The flux of latent heat released when new crust is formed is sufficient to drive many high-temperature systems on a short-term basis, but circulating fluids also extract heat associated with lithospheric cooling. Hydrothermal rebound following the end of ridge-crest circulation could extend to tens of kilometers off axis and, if neglected, may lead to overestimates of ridge-flank hydrothermal fluxes within young seafloor, but also might provide a way to evaluate the depth of advective cooling near the ridge. Fluid residence times within high-temperature hydrothermal systems based on geophysical considerations are on the order of years, consistent with geochemical estimates. Borehole observations suggest that basement permeabilities are very high locally within both ridge-crest and ridge-flank hydrothermal systems (10^{-9} to 10^{-10} m^2), but several lines of reasoning indicate the likely importance of anisotropy and heterogeneity in restricting most fluid flow to occur within a small fraction of rock. Future advances based on geophysical methods and modeling will result from *in situ* experiments and observations and interdisciplinary approaches that focus on the nature of fluid pathways, the size of hydrothermal reservoirs, and the coupling among physical, chemical, and geological dynamics.

Energy and Mass Transfer in Marine Hydrothermal Systems
Edited by P.E. Halbach, V. Tunnicliffe, and J.R. Hein
ISBN 3-934504-12-4 To order book, contact: dahlemup@zedat.fu-berlin.de

INTRODUCTION

Seafloor hydrothermal systems move enormous quantities of energy and mass between the lithosphere and hydrosphere, influence the physical and chemical state of the crust and overlying ocean, and support remarkable biological communities within and below the seafloor. Much of what we know about seafloor hydrothermal activity, and the overall nature of lithosphere creation and evolution, has come from geophysical experiments. These are defined broadly to include results of passive and active investigations in which physical conditions and properties within the lithosphere are measured or estimated using indirect techniques. In this chapter I describe selected historical developments and results of recent experiments and models having implications for heat and mass transfer from marine hydrothermal systems, discuss the energetics of these systems, and suggest how future studies may help to resolve remaining questions. Length and format limitations preclude a comprehensive overview of any of these topics (or thorough citation of references), so I focus instead on a small number of examples.

Geophysical approaches offer many advantages for studies of lithospheric heat and mass transfer. These approaches provide information about the physical state of the crust and upper mantle in areas where direct examination is not possible. In contrast to observations made on individual samples collected from the seafloor or shallow boreholes, geophysical approaches may allow assessments of properties and processes over two, three, or four dimensions (including time). Geophysical methods can be applied at large lateral and depth scales, including scales exceeding the thickness of the oceanic crust. However, geophysical approaches also suffer from several important limitations. They generally do not measure directly the properties of fundamental interest; instead, geophysical experiments provide data that can be used to infer conditions. Each geophysical method has a length scale below which it offers limited or no resolution, and typically there is an inverse correlation between measurement length scale and resolution. Perhaps most importantly, because they often rely on inverse techniques for interpretation of systems that are underconstrained, many geophysical methods result in nonunique solutions. Given these advantages and limitations, geophysical tools are perhaps most useful in resolving the nature of seafloor hydrothermal systems when combined with geological and geochemical observations and insights provided by models.

STRUCTURE OF UPPER OCEANIC LITHOSPHERE

Construction and Evolution

Mature oceanic crust is generally 6–7 km thick and is highly layered, as inferred from early seismic studies (e.g., Raitt 1963) and comparison with ophiolites (e.g., Cann 1974; Moores and Vine 1971). Initial seismic studies identified a shallow layer of varying thickness having low P-wave velocities (1.5–2.0 km/s; seismic layer 1), a layer 1.0–2.0 km thick having higher velocities (~2.5–6.0 km/s; seismic layer 2), and a layer 3.0–4.0 km thick having even higher velocities (~6.5–7.5 km/s; seismic layer 3). These seismic layers are generally associated with a lithostratigraphy of sediments, extrusive basalts (pillows, flows, breccia) and intrusive basalts (sheeted dikes), and gabbro, although this last correlation may not always apply (e.g., Detrick et al. 1994). The Moho separates these crustal rocks from underlying peridotitic

mantle rocks, which have velocities on the order of 8.3 km/s. Later seismic studies demonstrated that seafloor velocity structure was better described by layers having different velocity gradients (e.g., Spudich and Orcutt 1980), and that mean values and gradients often varied along strike and, especially for shallow volcanic rocks, with lithospheric age (e.g., Houtz and Ewing 1976).

Although crust formed at fast-spreading and slow-spreading ridges generally achieves similar thickness and gross structure, formation processes differ significantly between these settings. The shallowest crust at fast-spreading ridges experiences rapid evolution close to the axis. Dikes penetrate to the seafloor and extrude flows and pillows (e.g., Delaney et al. 1998). Seismic velocities in the uppermost crust very close to the ridge axis tend to be relatively high compared to those only a few kilometers off axis (e.g., McClain et al. 1985), a transition thought to result from accumulation of volcanic extrusives and an increase in fracturing. Another feature common to many fast-spreading ridges is an axial reflector at a depth of 1–2 km (Figure 3.1), generally thought to represent the top of a melt lens. The limited cross-ridge extent of this reflector (usually no more than 3–4 km, and often < 2 km) suggests that the region of largely liquid magma below fast-spreading ridges may be similarly restricted, but the presence of a much larger low-velocity volume below the axial reflector (and extending to the Moho) is though to indicate a "mush" zone having a significantly greater extent (e.g., Dunn et al. 2000). Collectively, the melt lens and low-velocity volume locally supply the magma that forms the crust, playing the role of the "magma chamber" inferred from ophiolite and early thermal studies.

The occurrence of a melt lens only in the shallow crust would suggest that the lower crust is created by downward migration of crystalline material ("gabbro glacier" model; Nicolas et al. 1988). Other studies have suggested that there may be a second, deeper melt lens near the base of the low-velocity volume (e.g., Crawford et al. 1999) or several melt lenses distributed at various depths (e.g., Keleman et al. 1997) contributing to construction of the lower crust.

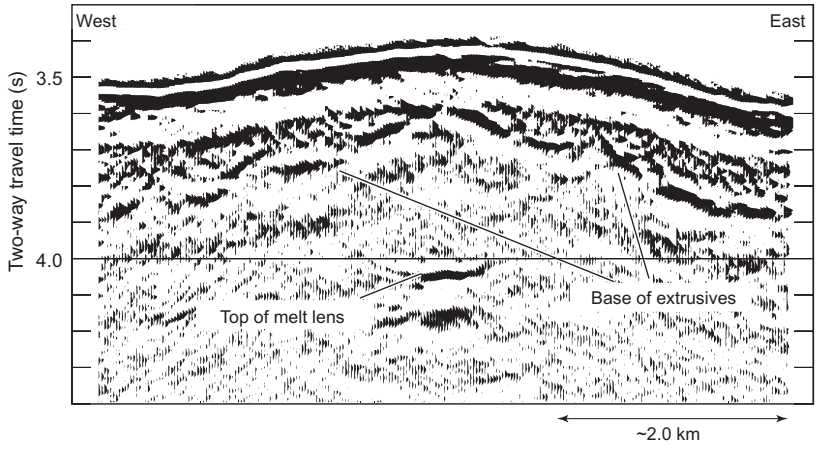

Figure 3.1 Migrated multichannel seismic profile across the East Pacific Rise at 9°40′ N (modified from Harding et al. 1993). Reflectors interpreted to represent the top of a melt lens and the base of the extrusive section are labeled.

The restricted width of the low-velocity volume down to the base of the crust (as determined from seismic tomography, Dunn et al. 2000), in contrast to conductive thermal models for lithospheric creation, suggests that advective heat loss may occur through the full thickness of the crust. This interpretation is consistent with evidence from ophiolites for hydration and hydrothermal cooling of the lower crust (Gregory and Taylor 1981), but not with most observations from *in situ* oceanic crust (see Alt and Bach, this volume). One possible way to reconcile these differing interpretations is that there is thermally significant fluid penetration into the deep crust, but that the fluid interacts geochemically with a small volume of rock.

Seismic studies also indicate the extent of variability along strike of the ridge, particularly variations in melt fraction associated with segment ends and other discontinuities (e.g., Detrick et al. 1987; Dunn et al. 2000). Melt lens reflections are common on fast-spreading ridges, but the large-scale correlation between these features and overlying, high-temperature hydrothermal systems is weak (e.g., Baker 1996). In addition, there is a general correlation between spreading rate and depth to magma lens reflection, with slower-spreading ridges having deeper reflections (Purdy et al. 1992).

Lithospheric creation processes are even more heterogeneous and transient at slow-spreading ridges, where along-strike differences in crustal thickness and thermal state (based mainly on gravity and seismic analyses) have been attributed to variations in melt supply from the mantle, with more robust supply to segment centers (e.g., Hooft et al. 2000; Lin et al. 1990; Purdy and Detrick 1986). Additional variability is contributed by tectonic unroofing and thinning of the crust, such that about 20% of seafloor spreading at slow-spreading centers results from lithospheric stretching (Solomon and Toomey 1992). Another important difference between slow- and fast-spreading ridges is the nature of seafloor bathymetry, with slow-spreading ridges having a characteristic median valley (generally tens of km wide, several km deep), and fast-spreading ridges having an overall axial high and locally a narrow, axial summit caldera. Slow-spreading ridges tend to have Bouguer gravity lows centered on the middle of first-order ridge segments, with deeper lows along longer segments (Lin et al. 1990). Upper crustal seismic velocities tend to increase rapidly with age for the first few million years, but velocities also tend to be lower, and individual seismic layers often are thinner, at segment edges (e.g., Detrick et al. 1993; Hosford et al. 2001). Seismic studies of slow-spreading ridges have rarely revealed shallow axial reflectors thought to indicate a melt lens (e.g., Sinha et al. 1997).

Crustal Seismicity

Several studies have used earthquakes to characterize the mechanical and thermal state of the oceanic crust close to the ridge. Huang and Solomon (1988) found a systematic correlation along ridges between the depths of large earthquakes and spreading rate: events tended to be deeper along slower-spreading ridges. This suggests a connection between thermal conditions at the ridge and the long-term rate at which melt is supplied, and perhaps an indication as to the depth extent of hydrothermal cooling (maintaining temperatures low enough to allow brittle failure). Larger earthquakes tend to be more common along ridge-segment ends than centers (Huang and Solomon 1988; Lin et al. 1990). Other studies of earthquake depths along the Mid-Atlantic Ridge (Kong et al. 1992; Toomey et al. 1988) demonstrated that events could be detected at or below the base of the crust where the magma budget was limited, but

that magmatically robust spreading segments tended to have shallower epicenters. Thus, magmatic and thermal conditions strongly influence ridge and near-ridge seismicity.

More recent work by Golden et al. (2003) in Middle Valley and Wilcock et al. (2003) along the Endeavour Segment, both on the northern Juan de Fuca Ridge, revealed microseismic activity at depths of 2–4 km below the seafloor. Microseismicity is interpreted in these studies to be associated with penetration of cool water into hot rock and subsequent extraction of crustal heat, consistent with the observation that swarms of events occur below active moderate- to high-temperature vent fields. The depth extent of these events is thought to indicate the depth of penetration of cold hydrothermal recharge, and some of the swarms define steeply dipping planes that run subparallel to the strike of the overlying ridge.

Two other recent studies have noted unexpected hydrogeologic responses to seismic events. Johnson et al. (2000a) documented abrupt changes in the temperature (and possibly volume flux) of low-temperature effluent at vent fields along the Endeavour Segment in 1999, 4–11 days following a swarm of earthquakes having a mean location about 8 km west of the ridge axis. This earthquake swarm is interpreted to be tectonic in nature and not associated with magmatic events. Sealed observatories installed in Ocean Drilling Program (ODP) boreholes on the eastern flank of the Juan de Fuca Ridge also detected changes in formation fluid pressure associated with individual earthquake events (along the Endeavour Segment to the west and the Nootka Fault to the north) over lateral distances of 20–100 km (Davis et al. 2001). These authors may also have detected an aseismic spreading event. Both of these studies suggest that hydrologic conditions respond to tectonic processes across distances of kilometers to tens of kilometers.

Studies of seismic anisotropy along ridges also have important implications for fluxes through seafloor hydrothermal systems. Crustal seismic velocities are expected to be influenced by the distribution and shape of fractures and pores, such that velocities will be faster along the long-axis directions of these features. Numerous researchers (e.g., Caress et al. 1992; Dunn and Toomey 2001; Sohn et al. 1997) have documented seismic velocities in the along-strike direction within the shallow subsurface of mid-ocean ridges that are on the order of 2–10% greater than velocities in the across-strike direction. If this anisotropy results from the orientation of hydrologically significant pores (e.g., faults and fractures), it suggests that fluid flow may be favored in an along-strike direction, an interpretation consistent with observations of vent field spacing, seismicity, and fluid chemistry along the Endeavour Segment (Delaney et al. 1992; Kelley, Delaney et al. 2001; Wilcock et al. 2003).

ENERGETICS OF HYDROTHERMAL SYSTEMS

Available Energy

There are three primary sources of energy available to drive hydrothermal circulation: the latent heat of crystallization as magma solidifies, heat released during cooling of magma and hot rock, and heat input at the base of the plate (referred to herein as latent heat, cooling heat, and basal heat, respectively). This categorization neglects recent discoveries of hydrothermal systems hosted by ultramafic rock and supported energetically (at least in part) by serpentinization (e.g., Kelley, Karson et al. 2001). Exothermic energy fluxes certainly are important locally, but we have little information at present to assess their global importance, and this potential heat source is neglected in the rest of the discussion.

Latent heat released during magmatic solidification will be concentrated where the lithosphere is created, mainly near seafloor spreading centers. Some ridge-flank areas may have short-term inputs of latent heat from off-axis volcanism, but these sites are likely to be spatially and temporally rare, except near actively forming oceanic islands or large igneous provinces. It is thought that magmatic inputs at slower-spreading ridges may be distributed both spatially (laterally and with depth) and temporally to a much greater extent than those along faster-spreading ridges (e.g., Hooft et al. 2000; Lin et al. 1990; Purdy and Detrick 1986; Solomon and Toomey 1992) but for the moment will consider all such inputs as occurring within a few kilometers of the spreading axis, and evaluate their cumulative impact over a sufficiently long time so as to justify the assumption of steady state conditions.

In contrast to latent heat, the release of heat associated with lithospheric cooling occurs both at the ridge crest and on ridge flanks, as upper lithosphere created at spreading centers loses a fraction of its initial heat. Efficient extraction of both kinds of heat by fluids requires penetration close to the heat source, but complete penetration by hydrothermal fluids is not essential, since conductive transport is enhanced by thinning of the conductive boundary layer separating heat sources and convecting fluids (e.g., Wilcock and Delaney 1996).

Heat added at the base of the plate also influences fluid flow and lithospheric evolution. This term is often neglected during consideration of ridge-crest hydrothermal systems, but it could play a significant role in places, and at times, of low magmatic input. Basal heat is likely to be the primary energy source driving hydrothermal circulation within older ridge flanks. One way to consider these different heat sources is that cooling and latent heat are both "advective inputs" at the ridge crest, since they are associated with the emplacement of new magma (creation of the plate) and subsequent cooling of crustal rocks. In contrast, basal heat input is a "conductive input" that occurs separate from magmatic intrusion, from the ridge crest to the subduction zone.

The latent, cooling, and basal heat sources available to drive hydrothermal circulation at steady state can be summarized as:

$$Q_{tot} = Q_{latent} + Q_{cooling} + Q_{basal} \tag{3.1a}$$

$$Q_{tot} = bu_{full}\,\rho\,(L + c_p\Delta T) - \overline{K} w_h \frac{dT}{dz} \tag{3.1b}$$

where Q = heat output per length of ridge along strike, b = vertical thickness of source layer, u_{full} = full spreading rate, c_p = crustal heat capacity, ΔT = mean temperature drop during cooling (from molten magma to solid crust), L = latent heat of solidification, $\overline{K}$ is the harmonic mean of thermal conductivity, w_h is the width perpendicular to the ridge over which basal input is considered, and dT/dz is the thermal gradient responsible for heat conduction into the base of the plate (temperature increasing with depth, requiring a negative sign so that heat flow is positive up).

The third term in Equation 3.1 is small relative to the other two and will be neglected for the remaining discussion of ridge-crest conditions. For example, model calculations suggest that close to the ridge axis this term will be about 80 mW/m^2 for a full spreading rate of 20 mm/yr, decreasing to 60 mW/m^2 within 1 Ma (see Figure A1 of Phipps Morgan and Chen 1993). Basal heat input values may be considerably higher at greater rates of spreading, but should be small compared to those associated with the release of latent and cooling heat.

An upper estimate of the steady state heat output at a mid-ocean ridge is generated by assuming vertical thickness equal to the mean crustal thickness of 6 km, and assuming reasonable values for other parameters (u_{full} = 10 to 150 mm/yr, ρ = 3000 kg/m^3, $c_p = 1.2 \times 10^3$ J/kg-K, $L = 6.8 \times 10^5$ J/kg, ΔT = 850°C) (Figure 3.2a). Cooling and latent heat components have about the same magnitude, with cooling heat being slightly greater on average. Comparison of these calculated values with estimates of heat output from individual vent fields and ridge segments, 100's to 1000's of MW (e.g., Baker 1996; Baker and Urabe 1996; Humphris and Cann 2000), confirms that there is generally insufficient heat available to maintain high-temperature vent fields at steady state unless heat is brought in from a considerable distance along strike.

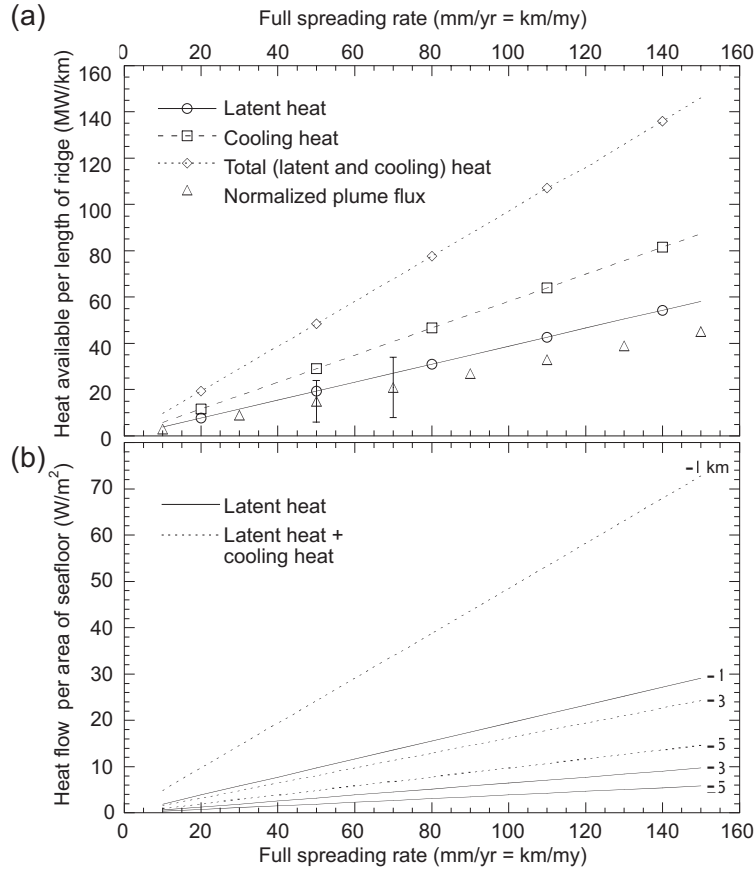

Figure 3.2 Ridge-crest heat output at steady state based on cooling and latent heat of solidication of a 6 km-thick layer of oceanic crust (Equation 3.1). (a) Heat output per length of ridge. Normalized plume flux values are from Baker et al. (1996). (b) Heat flow (flux per area) calculated from values in Figure 3.2a, assuming that heat is lost from area ±1, 3, or 5 km from the ridge axis, per length of ridge, as labeled.

However, there is no geophysical or hydrogeologic requirement that the heat supporting high-temperature venting must be obtained locally. There is geochemical and geophysical evidence from ridge-flank areas for thermally rapid fluid flow across distances of tens of kilometers or more (e.g., Baker et al. 1991; Davis et al. 1999), and lateral flow at a scale of kilometers has been documented in Middle Valley (e.g., Davis and Fisher 1994; Stein and Fisher 2001). Vent fluids from the northern end of the Endeavour Segment having a composition indicative of interaction with sediments at high temperatures (Butterfield et al. 1997; Lilley et al. 1993) could be explained by lateral flow over a considerable distance from the north, although the more conventional explanation is that the observed chemistry results from interaction with intercalated sediments at depth.

Baker et al. (1996) estimated vent field heat output from ridges around the world based on plume studies. They calculated the proportion of axial length over which venting has been documented, and assumed that the current spatial distribution can be considered to be a proxy for the temporal distribution. This allowed calculation of normalized, steady state hydrothermal heat output as a function of spreading rate, $\overline{H_a}$. Interestingly, calculated $\overline{H_a}$ values are close to the steady state latent heat output associated with solidification of a 6 km-thick crustal section (Figure 3.2a).

One possible interpretation of this observation is that high-temperature hydrothermal activity can be supported entirely by the latent heat of crustal solidification, leaving crustal cooling and basal heat input to drive lower-temperature ridge-crest and ridge-flank circulation (e.g., Humphris and Cann 2000; Lister 1981). However, fluids circulating into the crust in response to the release of latent heat cannot distinguish between this source and cooling heat. Both heat sources are abundant near spreading centers and both require fluid penetration for efficient, advective extraction. In fact, tomographic studies suggest that both kinds of heat are removed from full crustal depths close to the ridge (e.g., Dunn et al. 2000). Thus it seems likely that both heat sources (latent, cooling) supply significant fractions of the heat that drives ridge-crest circulation. The abrupt release of latent heat associated with solidification of newly injected magma may initiate or invigorate hydrothermal circulation, but once active, this circulation will extract heat as a function of fluid and crustal properties. The circulating fluid does not distinguish between the nature of heat sources.

Another implication of the correlation between spreading rate and hydrothermal output is that greater long-term fluxes of latent heat at fast-spreading ridges could allow individual high-temperature hydrothermal fields to be supported mainly by this heat source. Frequent magma injections at fast-spreading ridges would bring heat sources close to the seafloor near the axis, where their heat could be extracted rapidly and efficiently, but high advective heat fluxes documented at vent fields on intermediate- and slow-spreading ridges may draw a much greater fraction of their energy from cooling rock, requiring greater depth of penetration and more extensive lateral flow. This interpretation is consistent with the observed correlation between geochemically inferred water/rock ratios of ridge-crest hydrothermal systems and seafloor spreading rate (Bach and Humphris 1999), if fluids flowing within slower-spreading ridges travel greater lateral distances on average. Such a scenario is also consistent with both the tectonic control on venting commonly inferred at slow- and intermediate-spreading ridges, and the overall global distribution of high-temperature vent plumes, with fewer vent sites per ridge length on slower-spreading ridges (Baker 1996). This last scenario has important implications for thermal rebound on ridge flanks following the end of ridge-crest circulation, as discussed later in this chapter.

High versus Low Temperatures, Ridge Crest versus Ridge Flank

Ridge-crest hydrothermal systems vent fluids having a range of temperatures, but quantifying the fraction of heat lost thorough various mechanisms and temperatures is difficult (e.g., Elderfield and Schultz 1996). Studies of individual vent fields have suggested that 90% of the advective heat loss may be due to diffuse, low-temperature discharge (e.g., Murton et al. 1999; Schultz et al. 1992). Stein and Fisher (2001) estimated a 1:1 partitioning between conductive and advective heat loss across the 15 km-width of Middle Valley. This sedimented-ridge setting is unusual in that advective exchange between the crust and ocean is greatly restricted by a thick sediment layer, yielding what is likely a lower limit on the fraction of advective loss at bare-rock systems. It is difficult to assess the extent of heat loss, particularly conductive and low-temperature advective, along sections of ridges that are not presently hosting high-temperature hydrothermal circulation. It seems unlikely that advective heat loss ever stops completely within highly fractured and porous basement rocks exposed at the seafloor and heated from below, but the efficiency of this "background" cooling and its influence on lithospheric heat budgets are not known.

Lister (1981) distinguished between active and passive hydrothermal systems. The former were defined in places where cold fluid penetrates the rock through generation of a cracking front by thermal contraction, and the latter were described where flow was driven through previously cracked rock by conductive heating from below. This categorization neglects cracks formed by tectonic or magmatic processes and combines heat released by plate cooling and heat conducted through the plate from below. In their reexamination of plate cooling models based on global bathymetric and heat flow data, Stein and Stein (1992, 1994) distinguished between near-ridge and ridge-flank heat loss, noting that of the 1/3 of oceanic lithospheric heat loss that is advective, 70% of this advection is from seafloor > 1 Ma in age. It is not possible to resolve the fraction of advective heat loss from seafloor < 1 Ma in age based on conductive heat flow observations because these are difficult to make on bare rock, and it is not clear what reference should be used for comparison. Figure 3.2b shows steady state heat flow derived from latent and cooling sources within a few kilometers of the ridge crest as a function of spreading rate. Although the region of active magmatic intrusion is probably relatively narrow at fast-spreading ridges, the neovolcanic zone could be considerably wider at intermediate- and slow-spreading ridges, making it difficult to assess whether heat output at a particular site is above or below steady state values.

Ridge-flank hydrothermal circulation is known to be responsible for measurable advective heat loss from the lithosphere out to 65 Ma, on average (Stein and Stein 1992, 1994). Heat flow surveys have documented evidence of continued circulation, restricted to basement, at sites 80–105 Ma in age (e.g., Embley et al. 1983; Noel 1985). Fluid flow and heat advection in these systems are driven by plate cooling (on young ridge flanks) and heat input at the base of the plate (on young and older ridge flanks), except in rare locations where mid-plate volcanism adds additional latent and cooling heat. Ridge-flank circulation advects enormous heat fluxes on a global basis, but estimates of energy output from individual vent sites are rare (e.g., Mottl et al. 1998).

The preceding analyses neglect thermal input to the plate, and subsequent cooling, associated with off-axis volcanism. These fluxes are likely to be significant for short periods and within specific environments. However, on a global basis, at steady state, off-axis volcanism is unlikely to compare in magnitude to that required to construct the crust close to the ridge.

Thermal Transition from Ridge-crest to Ridge-flank Circulation

One difficulty with assessing the significance of ridge-crest versus ridge-flank advective heat fluxes is knowing where the transition between these systems occurs, and what reference should be used for comparison with observations. One-dimensional plate and thermal boundary models do not apply close to the ridge crest, and none includes the effects of hydrothermal circulation. Two-dimensional thermal models of lithospheric creation and evolution have taken two broad approaches to representing hydrothermal heat loss. One approach is to increase the efficiency of cooling, assumed to occur by hydrothermal circulation, by increasing the thermal conductivity of the shallow crust (e.g., Chen and Phipps Morgan 1996; Phipps Morgan and Chen 1993). Models are run with different cooling efficiencies, as denoted with the Nusselt number (the ratio of advective heat loss to conductive loss that would occur in the absence of advection) until a match is found between model output and observations (typically, the depth and general shape of a magma lens at the ridge crest). Another approach is to place heat sinks of differing magnitudes at various depths and distances from the ridge crest (e.g., Morton and Sleep 1985; Wilson et al. 1988). Because workers with both kinds of models have focused on the depth of the magma lens and the temperature structure close to the ridge axis, the thermal structure of the lithosphere away from the ridge axis has not received much attention in these studies.

In fact, thermal structure adjacent to and away from the ridge crest may tell us something about processes closer to the ridge and could also influence the magnitude of ridge-flank fluxes and our ability to estimate these values. A set of analytical calculations illustrate these points. Calculations are based on a one-dimensional, two-layer model of the upper oceanic lithosphere: a top layer that is cooled hydrothermally with 100% efficiency (such that it is at a temperature of 0°C relative to that of the overlying bottom water), and a deeper layer that conducts heat into the upper layer at a constant rate, q_0. Conductive heat flow out of the top of the upper layer (seafloor) after the end of hydrothermal cooling can be calculated as a function of time, upper layer thickness, and thermal properties (corrected from Hobart et al. 1985):

$$\frac{q}{q_0} = 2\sum_{n=0}^{\infty}(-1)^n \operatorname{erfc}\left(\frac{(2n+1)L}{2\sqrt{\kappa t}}\right) \tag{3.2}$$

where q/q_0 is the fraction of heat flow into the base of the upper layer that exits the top of the layer, L is upper layer thickness, and κ is thermal diffusivity. This formulation neglects lateral heat flow in the rebounding layer, much like one-dimensional plate and cooling half-space models used to derive standard curves for cooling oceanic lithosphere. Figure 3.3 shows how rebound is expected to vary with lithospheric age after the end of ridge-crest circulation. Initial suppression (and subsequent rebound) will be lower in magnitude if hydrothermal circulation is not 100% efficient, but the shapes of the curves should be about the same.

The extent of rebound at a given time scales with layer thickness. If only the upper 1–2 km of the crust are hydrothermally cooled close to the ridge axis, rebound to 90% of basal heat input occurs within 0.05–0.2 Ma. If most latent heat is released near the top of a melt lens within the shallow or mid-crust, and if this heat is the main energy source for ridge-crest hydrothermal activity, then rapid rebound is expected. However, if cooling penetrates to 4–5 km depth (e.g., Dunn et al. 2000), 90% rebound requires 0.7–1.0 Ma and could extend tens of kilometers off axis, depending on spreading rate.

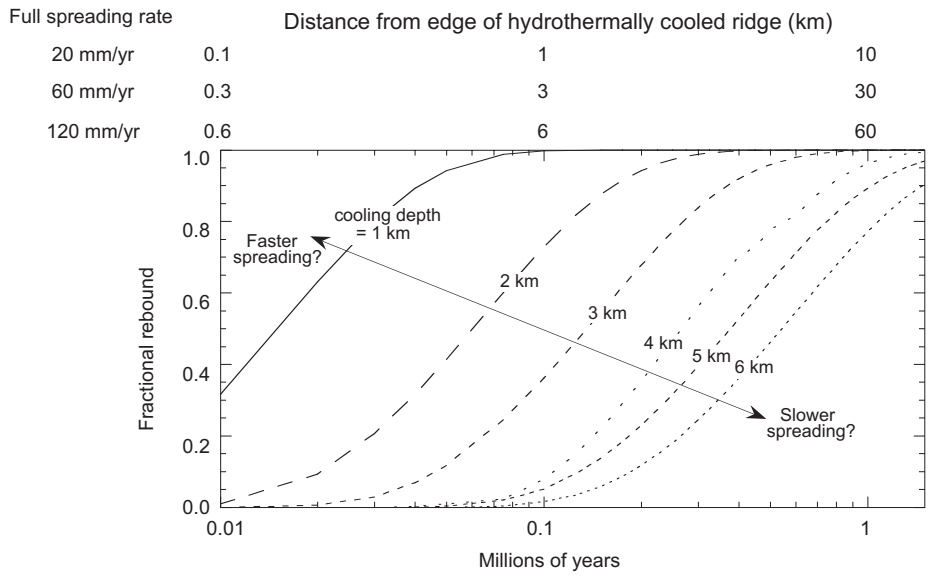

Figure 3.3 Calculated hydrothermal rebound following the end of high-temperature hydrothermal circulation at ridge crests, based on a one-dimensional model that assumes 100% efficiency in hydrothermal cooling (Equation 3.2). Lines are labeled with depth of hydrothermal cooling. Some geophysical observations suggest that the depth of hydrothermal circulation may be greater at slower-spreading ridges, causing rebound to occur later for slower-spreading ridges (as depicted with arrow on plot and discussed in the text), but other observations are consistent with deep hydrothermal cooling at fast-spreading ridges.

I have combined these calculations with estimates of total lithospheric heat output based on two-dimensional thermal models (Chen and Phipps Morgan 1996) to illustrate how thermal rebound could be expressed within young ridge flanks (Figure 3.4). Total heat output values (q_0) were taken from their models for seafloor spreading at full rates of 20, 60, 100, and 160 mm/yr (their Figure 1). In a primary set of calculations, I assumed that the depth of circulation scales with spreading rate, much as the depth to the top of a magma lens and the depth of seismicity scales with spreading rate (as discussed below, e.g., Kong et al. 1992; Purdy et al. 1992; Wilcock et al. 2003), using depths of 5.0, 2.7, 1.5, and 1.0 km, respectively, for the spreading rates listed above. This assumption does not imply that across-strike fluid circulation is more common within slower-spreading crust. Instead, along-strike circulation may occur across a broader region because of more extensive faulting, subparallel to strike, within slower-spreading crust.

I also assumed that the lateral extent of high-temperature circulation is the same as the vertical extent, such that the width of the hydrothermally cooled interval near the ridge is greater for slower spreading. This assumption contrasts with that implicit in Figure 3 of Chen and Phipps Morgan (1996) and Figure 1C of Baker et al. (1996). In those studies, hydrothermal heat loss as a function of spreading rate is assessed at a fixed distance from the ridge (± 1 or ± 2 km) or out to a fixed age (0.1 or 0.2 Ma). Using a fixed distance means that slower-spreading seafloor is cooled to younger ages than faster-spreading seafloor, and using a fixed age

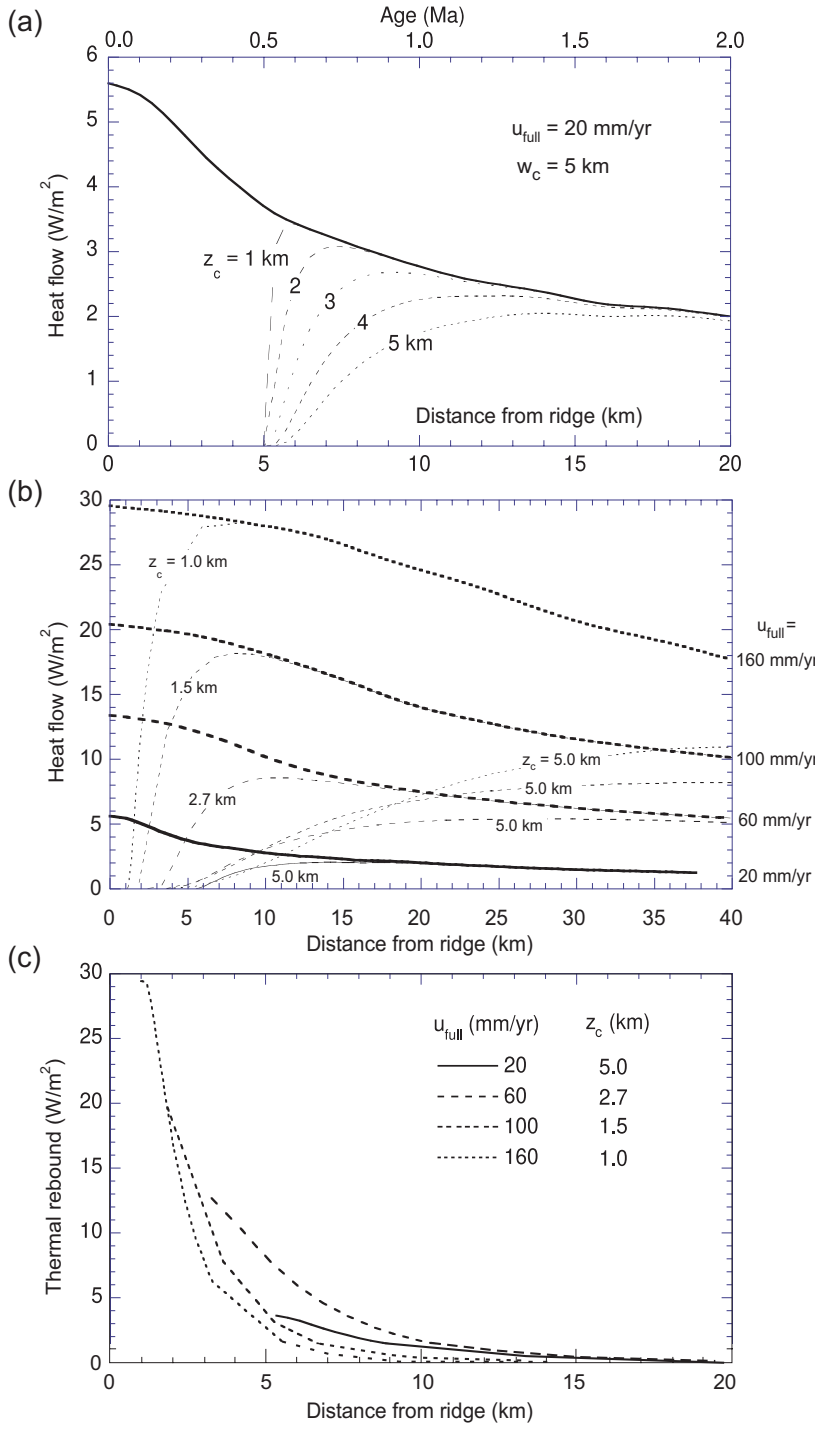
(a)
Age (Ma)
0.0
0.5
1.0
1.5
2.0
Heat flow (W/m2)
u full = 20 mm/yr
w c = 5 km
z c = 1 km
2
3
4
5 km
Distance from ridge (km)
(b)
Heat flow (W/m2)
z c = 1.0 km
1.5 km
2.7 km
5.0 km
z c = 5.0 km
5.0 km
5.0 km
u full =
160 mm/yr
100 mm/yr
60 mm/yr
20 mm/yr
Distance from ridge (km)
(c)
Thermal rebound (W/m2)
u full (mm/yr)
z c (km)
20
5.0
60
2.7
100
1.5
160
1.0
Distance from ridge (km)

results in a wider area of seafloor being cooled along faster-spreading ridges. In contrast, greater tectonism and depth of cooling along moderate- to slow-spreading ridges could lead to a longer time for thermal rebound (Figure 3.3).

For calculations based on greater depth and width of hydrothermal cooling for slower-spreading ridges, thermal rebound occurs within 10–20 km of the ridge axis (Figure 3.4a). Assuming a spreading-rate dependence on cooling width and depth, there is a trade-off with spreading rate such that the rebound versus distance behavior is similar for different spreading rates (Figure 3.4b and c). On the other hand, if ridge-crest hydrothermal fluids efficiently cool the crust to depths of 5 km for a range of spreading rates, there should be a measurable difference in heat available to drive ridge-flank circulation between slow-spreading and fast-spreading ridges (Figure 3.4b).

These calculations consider only cooling and rebound from ridge-crest hydrothermal circulation, neglecting entirely the initiation of ridge-flank circulation. If the transition between ridge-crest and ridge-flank circulation occurs within the same interval over which rebound from the effects of ridge-crest circulation occurs, it may not be possible to distinguish between these distinct processes. As a result, estimates of the magnitude of ridge-flank circulation may overstate advective fluxes because apparent anomalies are calculated through comparison of observations from young seafloor and results of one-dimensional, cooling plate calculations that do not include hydrothermal rebound. It may be possible to test this idea through careful heat flow surveys of young ridge flanks over a range of spreading rates, adjacent to ridge areas within which high-temperature circulation is both present and absent.

HYDROGEOLOGIC PROCESSES AND PROPERTIES

Hydrothermal Residence Times

Hydrologic reservoirs are sometimes considered in terms of their residence time, defined as the mass flux divided by reservoir mass (or volume flux/volume or heat flux/heat). The residence time concept applies to well-mixed systems at steady state. The consistency of the chemistry of some high-temperature vent fluids suggests that many of these systems operate

---

Figure 3.4 Combined lithospheric heat flow (Chen and Phipps Morgan 1996) and rebound calculations. (a) Total heat flow and calculated thermal rebound after the end of ridge-crest circulation as a function of the depth extent of hydrothermal cooling (z_c) for a slow-spreading ridge. The assumed width of the hydrothermally cooled region (w_c) is 5 km on either side of the ridge. Deeper cooling requires more time (and greater distance from the ridge) for recovery. (b) Calculated thermal rebound for four spreading rates and two depth-of-cooling scenarios. Lithospheric heat loss curves (bold lines) are from Chen and Phipps Morgan (1996, their Figure 1B) for different spreading rates. The total energy available to drive ridge-crest hydrothermal circulation scales with spreading rate. Rebound curves (thin lines) show the influence of lithospheric reheating on surface heat flow after ridge-crest hydrothermal circulation ends, for cases where the depth of cooling (z_c) scales with spreading rate (heat flow rebounds relatively quickly for moderate- to fast-spreading ridges) and cases where the depth of cooling is 5 km for all spreading rates (heat flow rebounds more slowly). The greatest spatial extent of thermal rebound is for fast spreading and deep circulation. (c) Magnitude of thermal rebound for cases in which the depth of cooling (z_c) scales with spreading rate (difference between total heat available, bold lines, and net heat flow during rebound, thin lines, in Figure 3.4b). The magnitude of the "missing heat", used to reheat the upper lithosphere after the end of ridge-crest hydrothermal circulation, is about the same for all spreading rates because of the trade-off between the rate of heat input and the depth of circulation.

at steady state, at least for several decades. Kadko and Moore (1988) and Kadko and Butterfield (1998) estimated fluid residence times geochemically within several high-temperature, seafloor hydrothermal systems. I have made independent estimates of residence times for these and similar systems based on measured heat output and calculated fluid volumes (heat capacities) (Figure 3.5). I assume that the volume of the hydrothermal reservoir, per kilometer along the ridge, is defined by the depth and width of hydrothermally active crust, based on the values used earlier for ridges spreading at 20–160 mm/yr (full rate), 5.0–1.0 km, respectively.

I assume an effective system porosity of 1–10%. The effective porosity differs from the total porosity in that the former includes only those pores that are well connected, the cracks and fractures through which most of the thermally significant flow occurs. I suspect that values closer to 1% are most likely to be appropriate for these calculations. The heat fluxes from high-temperature hydrothermal venting have been measured or estimated for numerous systems (e.g., Baker et al. 1996; Humphris and Cann 2000; Murton et al. 1999, and references therein). Heat flux is related to volume flux through consideration of the fluid density, heat capacity and mean temperature drop between the reaction zone and the seafloor (675 kg/m^3, 6400 J/kg-K, and 350°C, respectively), allowing estimation of residence times (Figure 3.5).

A reservoir size of $5 \times 10^8 - 5 \times 10^9$ m^3/km of ridge is estimated for a slow-spreading ridge (u_{full} = 20 mm/yr), and a considerably smaller reservoir size of $2 \times 10^7 - 2 \times 10^8$ m^3/km of ridge is estimated for a fast-spreading ridge (u_{full} = 160 mm/yr). Independent estimates of reservoir volumes, based on geochemical mass balance, are shown for the TAG and Middle Valley Bent Hill sulfide deposits (Figure 3.5). Also shown are estimates of instantaneous heat output for Broken Spur, Middle Valley, TAG, and Endeavour Segment vent fields, and normalized heat outputs for the global ridge system as a function of spreading rate. All of these estimates are consistent with steady state fluid residence times on the order of years within these systems (as opposed to weeks or decades), similar to geochemical estimates (Kadko and Butterfield 1998; Kadko and Moore 1988). These calculations may provide another explanation for the observation that hydrothermal fluids at slow-spreading ridges have chemistries indicative of more water–rock interaction (Bach and Humphris 1999): reservoir sizes and residence times may be greater at slow-spreading ridges.

Formation Hydrologic Properties

Some of what is known about the lithostratigraphy and hydrogeology of seafloor hydrothermal systems comes from borehole sampling and *in situ* testing. Borehole work is much easier in ridge-flank settings than in ridge-crest settings, but significant progress has been made in drilling ridge-crest hydrothermal sites in Middle Valley (Juan de Fuca Ridge) and TAG (Mid-Atlantic Ridge). Of these, only Middle Valley had a significant downhole measurement program within the underlying crust. Although sedimented spreading centers are significantly different from bare-rock ridges, we can draw inferences regarding the nature of ridge-crest hydrogeology from constraints provided by drilling and geophysical testing.

One of the most important parameters determining the amount of time hydrothermal fluids spend in contact with the lithosphere is permeability, a measure of the ease with which fluids move through the rock. Stein and Fisher (2001) used data from two boreholes in Middle Valley to estimate bulk hydrologic properties below an active, moderate-temperature (280°C)

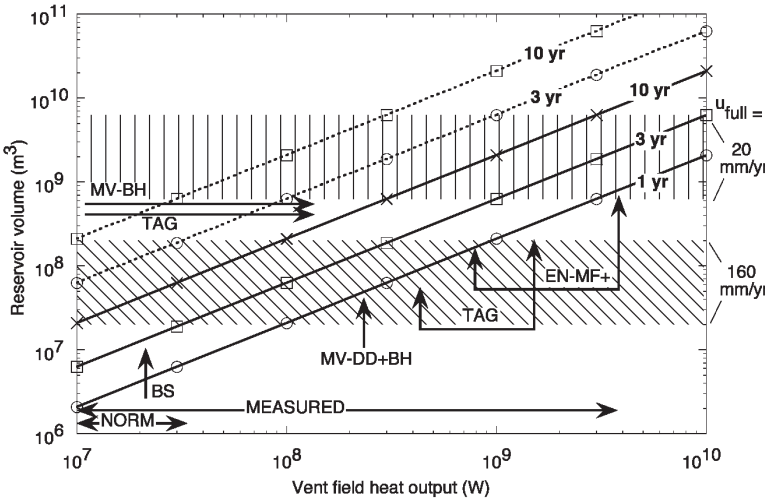

Figure 3.5 Calculations and estimates of ridge-crest hydrothermal reservoir volumes and heat output, related by fluid residence time. Estimated reservoir volumes per km of ridge crest were calculated for seafloor spreading full rates of 20 mm/yr to 160 mm/yr (labeled horizontal bands), based on hydrothermal circulation depths of 5.0 and 1.0 km, respectively, and effective porosity of 1–10%. Volumes for spreading rates between these extremes would fall between the two bands. Estimates of reservoir volumes needed to produce massive sulfide deposits are labeled with horizontal arrows for TAG and Middle Valley-Bent Hill (MV-BH). Vent field heat flow estimates are from Baker et al. (1996), Murton et al. (1999), Humphris and Cann (2000), and references therein, for Broken Spur (BS), Middle Valley-Dead Dog and Bent Hill (MV-DD+BH), TAG, and the Endeavour Segment, including the Main Field and other vent fields (EN-MF+). The heat output range labeled NORM indicates normalized high-temperature vent field output (correcting for the fraction of ridge hosting high-temperature circulation at any time, Baker et al. 1996) and the range labeled MEASURED indicates the total range of measured values for individual vent fields over all spreading rates. Diagonal lines are fluid residence times based on these values and assuming steady state conditions. Solid lines are for an effective porosity of 1%, and dashed lines are for an effective porosity of 10%. Ten-year residence time with effective porosity of 1% is equivalent to one-year residence time with effective porosity of 10%.

vent field. Two holes were cased and sealed in Middle Valley during ODP Leg 139, establishing the first CORK (sealed, seafloor) observatories (Davis and Becker 1994). Hole 858G was drilled in the Dead Dog vent field, within a few tens of meters of several clusters of active chimneys discharging fluids at temperatures up to 280°C. The hole penetrated 260 m of sediment and 175 m of basaltic basement, interpreted to be a buried volcanic edifice. Hole 857D was drilled 1.6 km south of the Dead Dog vent field through 470 m of sediments and 500 m of alternating sediments and sills, with this deeper section thought to include a part of the hydrothermal reservoir. Geophysical and flow-meter logs and packer experiments were completed, and both holes were sealed and instrumented (with thermistor chains, fluid samplers, and pressure gauges) and left to equilibrate. The observatories were visited by submersible and remotely operated vehicles over several years, and reinstrumented during a later ODP expedition.

Pressure records downloaded from the CORKs after 14 months (Davis and Becker 1998) suggested that basement fluids in Hole 858G were overpressured relative to seafloor hydrostatic conditions by 180 kPa, while fluid pressures in Hole 857D were underpressured by 400

kPa. This pattern makes some sense, since basement fluids in an area of active venting should be overpressured, and the fluids within the reservoir need to be underpressured in order to draw recharge. But this distribution of under- and overpressures also seems to suggest that fluids within basement should flow away from the vent field at depth. In fact, the *in situ* gradient in the fluid impelling force is from the reservoir area (Hole 857D) towards the vent field (Hole 858G), as determined by correcting the seafloor pressures measured at the observatories for differences in fluid temperature and density with depth (Stein and Fisher 2001). Based on the assumption that vigorously convecting fluids at depth are isothermal at 280°C, the temperature-corrected difference in pressure head between the two sites is only 1.7 m. This remarkably small head difference between sites 1.6 km apart suggests that hydrothermal basement in this area must be extremely permeable.

An estimate of large-scale basement permeability was made for this region based on application of a technique most commonly applied to pumping wells on land. Holes 858G and 857D are considered to be observation wells located 50 m and 1600 m, respectively, from the "pumping well" (the entire active Dead Dog vent field). Based on the temperature-corrected head difference between the observation points, and a range of aquifer thicknesses of 10–1000 m, the bulk permeability in basement necessary to supply fluid to the vents is 10^{-12} to 10^{-10} m^2, with the higher permeability value corresponding to the thinner aquifer. These values have large uncertainties, particularly because the pressures on the CORKed boreholes had not stabilized completely after 14 months of equilibration, but a bulk permeability of 10^{-10} m^2 was also estimated for a 5–10 m-thick interval at Site 857 based on packer and flow-meter experiments and other observations (Becker et al. 1994).

Measurements of permeability in the upper crust have been completed within several boreholes using packer and flow-meter methods, yielding a consistent set of observations over a range of depths and lithospheric ages (Becker and Fisher 2000; Fisher 1998). These experiments suggest that the highest bulk permeabilities, on the order of 10^{-10} to 10^{-13} m^2, tend to be found within the upper few hundred meters of basalt extrusives, and the greatest permeabilities are found within thin zones on the order of a few meters to tens of meters thick. Permeability is several orders of magnitude lower at greater depths into basement.

Fisher and Becker (2000) compared the permeability data from the upper 100 m of basaltic ocean crust to global compilations of ridge-flank seismic and heat flow data, and I have added a summary of bulk density estimates to this compilation (Figure 3.6). These data were collected from crust produced over a wide range of spreading rates, and although the data sets are generally too small to allow comparison of trends for different spreading rates, consistency of the complete data sets suggests that the observations may be independent of the rate of plate production. Global seismic data show a generally monotonic increase in velocities (from 2.5 to 4.5 km/s) within uppermost basement over the first 5 to 10 Ma of crustal evolution, followed by very slow or little change in velocities during subsequent aging (Figure 3.6a and b). The global data do not show the decrease in shallow velocities associated with volcanic construction and fracturing that have been documented very close to the ridge (e.g., McClain et al. 1985) because of coarse binning. Borehole permeability data show a trend consistent with the seismic data, with values of 10^{-10} m^2 for the youngest normal seafloor (not at a sedimented ridge) decreasing with age to about 10^{-14} m^2 after about 7 Ma. There is a large and unfortunate age gap in the ridge-flank permeability data between these data and those from some of the oldest remaining seafloor (Figure 3.6c), but it seems unlikely that bulk

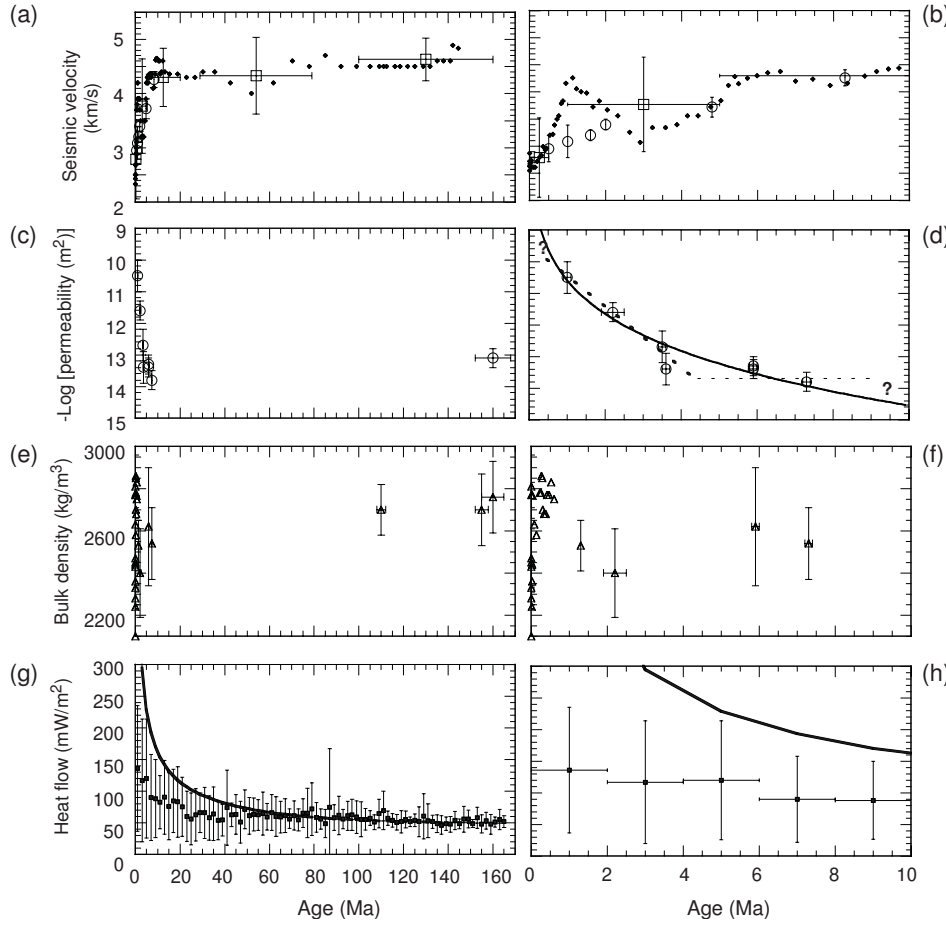

Figure 3.6 Properties of the upper oceanic crust and conductive heat loss from oceanic lithosphere compiled by age. Figure modified from Fisher and Becker (2000). All data sources are cited in that work, except for density data, which are from Johnson et al. (2000b) and references therein (seafloor gravity measurements) and Initial Reports volumes of the ODP (borehole lithodensity logs in the upper 100 m of basaltic crust). (a) Seismic velocities, 0–170 Ma. Horizontal error bars show the range of values used for group means, and vertical bars show± 1 standard deviation. (b) Seismic velocities, 0–10 Ma. (c) Permeabilities, 0–170 Ma. Horizontal bars show uncertainty in basement age; vertical bars show uncertainty in bulk permeability estimates, generally one order of magnitude. (d) Permeabilities, 0–10 Ma. Straight lines and curve indicate possible trends. (e) Bulk densities, 0–170 Ma. Horizontal bars in borehole data are uncertainties in basement ages; vertical bars indicate one standard deviation of values from upper 100 m of basement. (f) Bulk densities, 0–10 Ma. (g) Heat flow, 0–170 Ma. Vertical bars show 1 standard deviation of binned data. (h) Heat flow, 0–10 Ma. Horizontal bars show range of age bins.

permeability could continue to decrease if ridge flanks are to host thermally significant convection out to 65 Ma on average (Stein and Stein 1992, 1994).

Estimates of bulk density within the shallowest seafloor were derived from two general sources: borehole lithodensity logs and seafloor gravity measurements (Figure 3.6e and f).

Lithodensity data are from measurements made in ODP drillholes, and gravity measurements are from *Alvin* surveys of ridge-crest and young ridge-flank environments (Johnson et al. 2000b and references therein). The gravity-based bulk density data show considerable scatter close to the ridge, but also suggest an overall rise in densities during the first 0.5 Ma from 2400 to 2800 kg/m^3. Ridge-flank bulk densities in seafloor aged 5 to 160 Ma generally increase from 2600 to 2800 kg/m^3, but there is considerable variability in data from individual boreholes, and it is not clear if the apparent decrease between 0.5 and 1.3 Ma is an artifact of different measurement types, resulted from tectonism along the Blanco Fracture Zone (where the 1.3 Ma data were collected), or represents a more universal process.

The observed magnitude of crustal permeabilities determined from direct testing in boreholes (Figure 3.6) contrasts sharply with values inferred from other methods that take a larger view of the upper lithosphere. In one recent experiment, Davis et al. (2000) inferred permeabilities for the upper crust on the order of 10^{-9} m^2 based on one-dimensional analytical models of formation pressure responses to tides in sealed basement boreholes. Fisher and Becker (2000) argued that, although shallow crustal permeability and seismic velocities were consistent with infilling of crustal pores with age as a result of ridge-flank hydrothermal convection, ridge-flank heat flow anomalies required considerably greater effective permeabilities in order to host sufficiently vigorous fluid flow. This interpretation was reconciled with a conceptual model in which most thermally significant fluid flow on ridge flanks occurs through a very small fraction of the rock, a process known as "flow channeling" (Tsang and Neretnieks 1998).

There is good evidence from geological, geochemical, and geophysical observations for the restriction of thermally significant fluid flow to occur within a small fraction of the upper lithosphere. For example, Alt (1995) shows whole rock geochemical analyses that reveal enormous heterogeneity in the extent of water/rock interaction within the upper 2 km (particularly the upper 500 m) of basement. As another example, Figure 3.7 shows a compilation of lithologic and three kinds of geophysical data from DSDP/ODP Hole 395A on the west flank of the Mid-Atlantic Ridge. Lithologic and electrical resistivity logs were compared by shipboard scientists after an initial phase of drilling and experiments and interpreted to indicate a series of vertically distinct, basaltic flows (Matthews et al. 1984). Each flow unit is characterized by greater electrical resistivity at the base and lower electrical resistivity at the top, interpreted to indicate an increase in porosity in rocks deposited during the final stages of each effusive event.

Temperature logs collected soon after drilling (Becker et al. 1984) indicated that bottom water was being drawn down Hole 395A at 10–100 m/hr because the formation pressure was less than that generated by a borehole filled with cold seawater, and this flow has continued for many years. Scientists returned to the hole in 1998 to conduct additional geophysical experiments, including recording of a spontaneous potential (SP) log in the open hole (Becker, Malone, et al. 1998). The SP tool is used commonly in oil wells to determine the locations of intervals within a borehole that receive or produce borehole fluid. Deflections in the Hole 395A SP log clearly correlate with the tops of individual resistivity sequences, suggesting that these thin intervals, previously interpreted based on lithologic and resistivity data to have higher porosity, are also the most hydrologically active intervals (Figure 3.7). The typical ratio in thicknesses of the most and least hydrologically active sections of this borehole is on the order of 1:10 to 1:100.

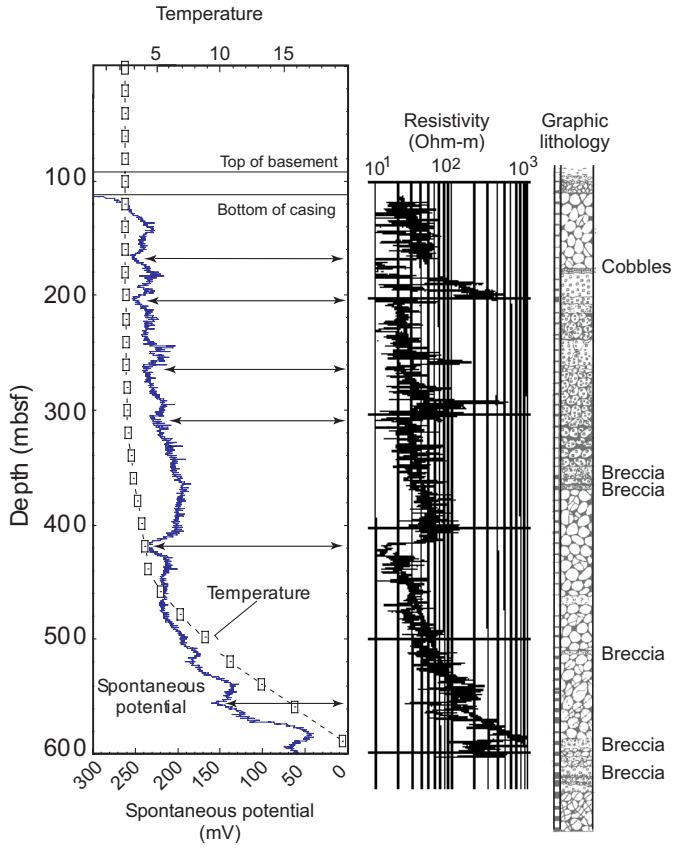

Figure 3.7 Comparison of lithology and geophysical log data from Hole 395A (Barletzko et al. 2001; Becker et al. 2001). Graphic lithology and resistivity data from Matthews et al. (1984). Resistivity-decreasing-up sequences (bold, dashed lines) interpreted to indicate individual effusive events, with greater porosity at the top. Temperature and spontaneous potential (SP) data from Becker et al. (1998). Concave-down temperature log indicates flow of cold bottom water into the open hole at depth. Deflections in the SP log interpreted to indicate locations of intervals into which water is being drawn into basement by differential pressure. Arrows illustrate one-to-one correlation between these intervals and tops of resistivity units, suggesting that these are the most hydrologically active intervals of the formation. Note relative thickness of these intervals compared to hydrologically less important intervals.

The importance of flow channeling at ridge crests is unknown, but within heterogeneous fluid–rock systems in general, fluid flow pathways favor the most permeable networks, even when overall system permeability is high (Moreno and Tsang 1994; Tsang and Neretnieks 1998). Thus even if bulk permeability within ridge-crest rocks is as great as suggested by some of the studies discussed earlier, most of the fluid flow could still be confined to a relatively small fraction of the rock. In combination with seismic anisotropy measurements described above, interpreted to indicate a preferential orientation of fractures and other pores, flow channeling in ridge-crest hydrothermal systems could result in considerably more fluid moving along strike than across strike, and in the along-strike direction, most fluid moving

within spatially restricted regions that include the largest and best-connected pathways. Flow channeling would greatly influence the efficiency of heat extraction from ridge-crest hydrothermal systems, but would be even more important for geochemical and biological fluxes and the separation of distinct fluid reservoirs within the upper lithosphere.

FUTURE OPPORTUNITIES

Geophysical experiments have provided critical information on the physical state and hydrothermal processes active within the upper oceanic lithosphere, but there remain significant gaps in our understanding. Many of these gaps can be addressed through interdisciplinary experiments that involve application of multiple methods in the same location, and through improvements in measurement, data storage, and analytical capabilities.

Perhaps the greatest gap in our knowledge of the physics of seafloor hydrothermal systems is the nature (origin, extent, orientation, connectedness, evolution) of the fluid pathways. Geophysical tools run from the seafloor offer limited means to assess these pathways at depth because of the indirect nature and degradation in resolution of surface measurements. As in heterogeneous and fractured aquifers on land, the most reliable measurements of hydrologic properties in the seafloor will come from direct, controlled experiments. Geophysical tools will be particularly useful in helping to eliminate unrealistic interpretations from these experiments, and in extending results spatially away from observation points. Simply delineating the thermal structure of the upper oceanic lithosphere, along and across strike, will help to resolve critical questions involving the depth and lateral extent and magnitude of fluid circulation.

Tomographic techniques have revolutionized interpretation of subseafloor seismic experiments, but have yet to be applied in a seafloor setting between basement boreholes. In combination with cross-hole hydrologic and geochemical tracer experiments, cross-hole geophysical techniques could provide critical constraints on the importance of individual fluid flow pathways and the efficiency of heat advection. Plume studies have helped to identify locations of active hydrothermal venting and to assess short-term budgets (fluid, chemical, thermal), but these studies will need to be repeated many times (perhaps through installation of permanent observatories) in order to resolve long-term versus short-term budgets. These measurements should be linked to natural variations in seismicity and magmatic events so that we can assess the fundamental controls on hydrothermal fluxes and links between related processes (seismicity, volcanism, vent discharge).

Another lingering challenge in high-temperature vent studies is determining how high-temperature systems are recharged, and the extent to which fluids recirculate at depth before returning to the surface. These questions may be addressed through long-term tracer and monitoring experiments. Our ability to understand the dynamics of hydrothermal circulation depends on making measurements across a range of spatial and temporal scales, and co-locating experiments so that we can combine observational constraints based on independent assumptions.

ACKNOWLEDGMENTS

Work leading to this paper was supported by NSF, ODP, and the LANL/CULAR program. A. Harding kindly provided the image for Figure 3.1, and W. Wilcock and C. Golden provided preprints of papers in

press. M. Hutnak provided editorial suggestions for an earlier version of this paper. Helpful comments and suggestions were provided by J. Alt, W. Bach, three anonymous reviewers, and numerous colleagues at the Dahlem Workshop.

REFERENCES

Alt, J.C. 1995. Subseafloor processes in mid-ocean ridge hydrothermal systems. In: Seafloor Hydrothermal Systems: Physical, Chemical, Biological and Geological Interactions, ed. S.E. Humphris, R.A. Zierenberg, L.S. Mullineaux, and R.E. Thompson, Geophys. Monograph 91, pp. 85–114. Washington, D.C.: Am. Geophys. Union.

Bach, W., and S.E. Humphris. 1999. Relationship between Sr and O isotope compositions of hydrothermal fluids and the spreading and magma supply rates at oceanic spreading centers. *Geology* **27**:1067–1070.

Baker, E.T. 1996. Geological indexes of hydrothermal venting. *J. Geophys. Res.* **101**:13,741–13,753.

Baker, E.T., Y.J. Chen, and J.P. Morgan. 1996. The relationship between near-axes hydrothermal cooling and the spreading rate of mid-ocean ridges. *Earth Planet. Sci. Lett.* **142**:137–145.

Baker, E.T., and T. Urabe. 1996. Extensive distribution of hydrothermal plumes along the superfast spreading East Pacific Rise, 13°30′–18°40′S. *J. Geophys. Res.* **101**:8685–8695.

Baker, P., P. Stout, M. Kastner, and H. Elderfield. 1991. Large-scale lateral advection of seawater through oceanic crust in the central equatorial Pacific. *Earth Planet. Sci. Lett.* **105**:522–533.

Barletzko, A., P. Pezard, D. Goldberg, Y.F. Sun, and K. Becker. 2001. Volcanic stratigraphy of DSDP/ODP Hole 395A: An interpretation using well-logging data. *Mar. Geophys. Res.* **22**:111–127.

Becker, K., A. Barletzko, and E.E. Davis. 2001. Leg 174B synopsis: Revisiting Hole 395A for logging and long-term monitoring of off-axis hydrothermal processes in young oceanic crust. In: Proc. Ocean Drilling Program (ODP), Sci. Results vol. 174B, ed. K. Becker and M.J. Malone, pp. 1–12. College Station, TX: ODP.

Becker, K., and A. Fisher. 2000. Permeability of upper oceanic basement on the eastern flank of the Endeavour Ridge determined with drill-string packer experiments. *J. Geophys. Res.* **105**:897–912.

Becker, K., M.G. Langseth, and R.D. Hyndman. 1984. Temperature measurements in Hole 395A, Leg 78B. In: Deep-Sea Drilling Project, Init. Repts. vol. 78B, ed. R. Hyndman and M. Salisbury, pp. 689–698. Washington, D.C.: U.S. GPO.

Becker, K., M.J. Malone et al. 1998. Cork Hole 395A, Leg 174B. Proc. Ocean Drilling Program (ODP), Init. Repts., vol. 174B. College Station, TX: ODP.

Becker, K., R.H. Morin, and E.E. Davis. 1994. Permeabilities in the Middle Valley hydrothermal system measured with packer and flowmeter experiments. In: Proc. Ocean Drilling Program (ODP), Sci. Results vol. 139, ed. E.E. Davis, M.J. Mottl, A.T. Fisher, and J.F. Slack, pp. 613–626. College Station, TX: ODP.

Butterfield, D.A., I.R. Jonasson, G.J. Massoth, R.A. Feely, K.K. Roe, R.E. Embley, J.F. Holden, R.E. McDuff, M.D. Lilley, and J.R. Delaney. 1997. Seafloor eruptions and evolution of hydrothermal fluid chemistry. *Phil. Trans. R. Soc. Lond. A* **355**:369–386.

Cann, J.R. 1974. A layered model for oceanic crust developed. *Geophys. J. R. Astr. Soc.* **39**:169 187.

Caress, D., M.S. Burnett, and J.A. Orcutt. 1992. Tomographic image of the axial low-velocity zone at 12°50′N on the East Pacific Rise. *J. Geophys. Res.* **97**:9243–9263.

Chen, Y.J., and J. Phipps Morgan. 1996. The effects of spreading rate, the magma budget, and the geometry of magma emplacement on the axial heat flux at mid-ocean ridges. *J. Geophys. Res.* **101**:11,475–11,482.

Crawford, W.C., S.C. Webb, and J.A. Hildebrand. 1999. Constraints on melt in the lower crust and Moho at the East Pacific Rise, 9°48′N, using seafloor compliance measurements. *J. Geophys. Res.* **104**:2923–2939.

Davis, E., and K. Becker. 1998. Borehole observations record driving forces for hydrothermal circulation in young oceanic crust. *EOS* **79**:369; 377–378.

Davis, E.E., and K. Becker. 1994. Formation temperatures and pressures in a sedimented rift hydrothermal system: 10 months of CORK observations, Holes 857D and 858G. In: Proc. Ocean Drilling Program (ODP), Sci. Results vol. 139, ed. E.E. Davis, M.J. Mottl, A.T. Fisher, and J.F. Slack, pp. 649–666. College Station, TX: ODP.

Davis, E.E., D.S. Chapman, K. Wang, H. Villinger, A.T. Fisher, S.W. Robinson, J. Grigel, D. Pribnow, J. Stein, and K. Becker. 1999. Regional heat-flow variations across the sedimented Juan de Fuca Ridge eastern flank: Constraints on lithospheric cooling and lateral hydrothermal heat transport. *J. Geophys. Res.* **104**:17,675–17,688.

Davis, E.E., and A.T. Fisher. 1994. On the nature and consequences of hydrothermal circulation in the Middle Valley sedimented rift: Inferences from geophysical and geochemical observations, Leg 139. In: Proc. Ocean Drilling Program (ODP), Sci. Results vol. 139, ed. E.E. Davis, M.J. Mottl, A.T. Fisher, and J.F. Slack, pp. 695–717. College Station, TX: ODP.

Davis, E.E., W. Wang, K. Becker, and R.E. Thompson. 2000. Formation-scale hydraulic and mechanical properties of oceanic crust inferred from pore-pressure response to periodic seafloor loading. *J. Geophys. Res.* **105**:13,423–13,435.

Davis, E.E., W. Wang, R.E. Thomson, K. Becker, and J.F. Cassidy. 2001. An episode of seafloor spreading and associated plate deformation inferred from crustal fluid pressure transients. *J. Geophys. Res.* **106**:21,953–21,963.

Delaney, J.R., D.S. Kelley, M.D. Lilley, D.A. Butterfield, J.A. Baross, W.S.D. Wilcock, R.W. Embley, and M. Summit. 1998. The quantum event of oceanic crustal accretion: Impacts of diking at mid-ocean ridges. *Science* **281**:222–230.

Delaney, J.R., V. Robigou, R. McDuff, and M.A. Tivey. 1992. Geology of a vigorous hydrothermal system on the Endeavour Segment, Juan de Fuca Ridge. *J. Geophys. Res.* **97**:19,663–19,682.

Detrick, R.S., P. Buhl, E. Vera, J.C. Mutter, J.A. Orcutt, J. Madsen, and T. Brocher. 1987. Multi-channel seismic imaging of a crustal magma chamber along the East Pacific Rise. *Nature* **326**:61–64.

Detrick, R.S., J. Collins, R. Steven, and S. Swift. 1994. *In situ* evidence for the nature of the seismic layer 2/3 boundary in oceanic crust. *Nature* **370**:288–290.

Detrick, R.S., A.J. Harding, G.M. Kent, J.A. Orcutt, J.C. Mutter, and P. Buhl. 1993. Seismic structure of the southern East Pacific Rise. *Science* **259**:499–503.

Dunn, R.A., and D.R. Toomey. 2001. Crack-induced seismic anisotropy in the oceanic crust across the East Pacific Rise (9°30′N). *Earth Planet. Sci. Lett.* **189**:9–17.

Dunn, R.A., D.R. Toomey, and S.C. Solomon. 2000. Three-dimensional seismic structure and physical properties of the crust and shallow mantle beneath the East Pacific Rise at 9°30′N. *J. Geophys. Res.* **105**:23,537–23,555.

Elderfield, H., and A. Schultz. 1996. Mid-ocean ridge hydrothermal fluxes and the chemical composition of the ocean. *Ann. Rev. Earth Planet. Sci.* **24**:191–224.

Embley, R.W., M. Hobart, R. Anderson, and D. Abbott. 1983. Anomalous heat flow in the northwest Atlantic, a case for continued hydrothermal circulation in 80 MY crust. *J. Geophys. Res.* **88**:1067–1074.

Fisher, A.T. 1998. Permeability within basaltic oceanic crust. *Rev. Geophys.* **36**:143–182.

Fisher, A., and K. Becker. 2000. Channelized fluid flow in oceanic crust reconciles heat-flow and permeability data. *Nature* **403**:71–74.

Golden, C.E., S.C. Webb, and R.A. Sohn. 2003. Hydrothermal processes induce seismicity at Middle Valley, Juan de Fuca Ridge. *J. Geophys. Res*., in press.

Gregory, R.T., and H.P. Taylor. 1981. An oxygen isotope profile in a section of Cretaceous oceanic crust, Samail Ophiolite, Oman: Evidence for $\delta^{18}O$ buffering of the oceans by deep (>5 km) seawater-hydrothermal circulation at mid-ocean ridges. *J. Geophys. Res.* **86**:2737–2755.

Harding, A.J., G.M. Kent, and J.A. Orcutt. 1993. A multichannel seismic investigation of upper oceanic crust at 9°N on the East Pacific Rise: Implications for crustal accretion. *J. Geophys. Res.* **98**:13,925–13,944.

Hobart, M., M. Langseth, and R.N. Anderson. 1985. A geothermal and geophysical survey of the south flank of the Costa Rica Rift, sites 504 and 505. In: Deep-Sea Drilling Project, Init. Repts., vol. 83, ed. R. Anderson, J. Honnorez, and K. Becker, pp. 379–404. Washington, D.C.: U.S. GPO.

Hooft, E.E.E., R.S. Detrick, D.R. Toomey, J.A. Collins, and J. Lin. 2000. Crustal thickness and structure along three contrasting spreading segments of the Mid-Atlantic Ridge, 33.5°–35°N. *J. Geophys. Res.* **105**:8205–8226.

Hosford, A., J. Lin, and R.S. Detrick. 2001. Crustal evolution over the last 2 m.y. at the Mid Atlantic Ridge OH-1 segment, 35°N. *J. Geophys. Res.* **106**:13,269–13,285.

Houtz, R., and J. Ewing. 1976. Upper crustal structure as a function of plate age. *J. Geophys. Res.* **81**:2490–2498.

Huang, P.Y., and S.C. Solomon. 1988. Centroid depths of mid-ocean ridge earthquakes: Dependence on spreading rate. *J. Geophys. Res.* **93**:13,445–13,477.

Humphris, S.E., and J.R. Cann. 2000. Constraints on the energy and chemical balances of the modern TAG and ancient Cyprus seafloor sulfide deposits. *J. Geophys. Res.* **105**:28,477–28,488.

Johnson, H.P., M. Hutnak, R.P. Dziak, C.G. Fox, I. Urcuyo, J.P. Cowen, J. Nabelek, and C. Fisher. 2000a. Earthquake-induced changes in a hydrothermal system on the Juan de Fuca mid-ocean ridge, *Nature* **407**:174–176.

Johnson, H.P., M.J. Pruis, D. Van Patten, and M.A. Tivey. 2000b. Density and porosity of the upper oceanic crust from seafloor gravity measurements. *Geophys. Res. Lett.* 2**7**:1053–1056.

Kadko, D., and D.A. Butterfield. 1998. The relationship of hydrothermal fluid composition and crustal residence time to maturity of vent fields on the Juan de Fuca Ridge. *Geochim. Cosmochim. Acta* **62**:1521–1533.

Kadko, D., and W. Moore. 1988. Radiochemical constraints on the crustal residence time of submarine hydrothermal fluids: Endeavour Ridge. *Geochim. Cosmochim. Acta* **52**:659–668.

Keleman, P.B., K. Koga, and N. Shimizu. 1997. Geochemistry of gabbro sills in the crust–mantle transition zone of the Oman ophiolite: Implications for the origin of the oceanic lower crust. *Earth Planet. Sci. Lett.* **146**:475–488.

Kelley, D.S., J.R. Delaney, and D.R. Yoerger. 2001. Geology and venting dynamics of the Mothra hydrothermal field, Endeavour Segment, Juan de Fuca Ridge. *Geology* **10**:959–962**.**

Kelley, D.S., J.A. Karson, D.K. Blackman, G. Früh-Green, D.A. Butterfield, M.D. Lilley, E.J. Olson, M.O. Schrenk, K.K. Roe, G.T. Lebon, and P. Rivizzigno. 2001. An off-axis hydrothermal vent field near the Mid-Atlantic Ridge at 30°N. *Nature* **412**:145–149.

Kong, L.S.L., S.C. Solomon, and G.M. Purdy. 1992. Microearthquake characteristics of a mid-ocean ridge along-axis high. *J. Geophys. Res.* **97**:1659–1685.

Lilley, M.D., D.A. Butterfield, E.J. Olson, J.E. Lupton, S.A. Macko, and R.E. McDuff. 1993. Anomalous CH_4 and NH_4^+ concentrations at an unsedimented mid-ocean ridge hydrothermal system. *Nature* **364**:45–47.

Lin, J., G.M. Purdy, H. Schouten, J.-C. Sempere, and C. Zarvas. 1990. Evidence from gravity data for focused magmatic accretion along the Mid-Atlantic Ridge. *Nature* **344**:217–225.

Lister, C.R.B. 1981. Active and passive hydrothermal systems in the oceanic crust: Predicted physical conditions. In: The Dynamic Environment of the Ocean Floor, ed. K.A. Fanning and F.T. Manheim, pp. 441–470. Lexington MA: D.C. Heath.

Matthews, M., M. Salisbury, and R. Hyndman. 1984. Basement logging on the Mid-Atlantic Ridge, Deep Sea Drilling Project Hole 395A. In: Deep Sea Drilling Project, Init. Repts. vol. 78B, ed. R.D. Hyndman and M.H. Salisbury, pp. 717–730. Washington, D.C.: U.S. GPO.

McClain, J.S., J. Orcutt, and M. Burnett. 1985. The East Pacific Rise in cross section: A seismic model. *J. Geophys. Res.* **90**:8627–8639.

Moores, E.M., and F.J. Vine. 1971. The Troodos massif, Cyprus, and other ophiolites as oceanic crust: Evaluations and implications. *Phil. Trans. R. Soc. Lond. A* **268**:443–466.

Moreno, L., and C.-F. Tsang. 1994. Flow channeling in strongly heterogeneous porous media: A numerical study. *Water Resour. Res.* **30**:1421–1430.

Morton, J., and N. Sleep. 1985. A mid-ocean ridge thermal model, constraints on the volume of axial hydrothermal heat flux. *J. Geophys. Res.* **90**:11,345–11,353.

Mottl, M.J., C.G. Wheat, E. Baker, N. Becker, E. Davis, R. Feeley, A. Grehan, D. Kadko, M. Lilley, G. Massoth, C. Moyer, and F. Sansone. 1998. Warm springs discovered on 3.5 Ma oceanic crust, eastern flank of the Juan de Fuca Ridge. *Geology* 2**6**:51–54.

Murton, B.J., L.J. Redbourn, C.G. German, and E.T. Baker. 1999. Sources and fluxes of hydrothermal heat, chemicals, and biology within a segment of the Mid-Atlantic Ridge. *Earth Planet. Sci. Lett.* **171**:301–317.

Nicolas, A., I. Reuber, and K. Benn. 1988. A new magma chamber model based on structural studies in the Oman ophiolite. *Tectonophysics.* **151**:87–105.

Noel, M. 1985. Heat flow, sediment faulting, and porewater advection in the Madeira anyssal plain. *Earth Planet. Sci. Lett.* **73**:398–406.

Phipps Morgan, J., and Y.J. Chen. 1993. The genesis of oceanic crust: Magma injection, hydrothermal circulation, and crustal flow. *J. Geophys. Res.* **98**:6283–6297.

Purdy, M., and R. Detrick. 1986. Crustal structure of the Mid-Atlantic Ridge at 23°N from seismic refraction studies. *J. Geophys. Res.* **91**:3739–3762.

Purdy, M., L.S.L. Kong, G.L. Christeson, and S.C. Solomon. 1992. Relation between spreading rate and the seismic structure of mid-ocean ridges. *Nature* **355**:815–817.

Raitt, R.W. 1963. The crustal rocks. In: The Sea, ed. M.N. Hill, vol. 3, pp. 85–102. New York: Wiley.

Schultz, A., J.R. Delaney, and R.E. McDuff. 1992. On the partitioning of heat flux between diffuse and point source seafloor venting. *J. Geophys. Res.* **97**:12,299–12,315.

Sinha, M., D.A. Navin, L.M. MacGregor, S. Constable, C. Peirce, A. White, G. Heinson, and M.A. Inglis. 1997. Evidence for accumulated melt beneath the slow-spreading Mid-Atlantic ridge. *Phil. Trans. R. Soc. Lond. A* **355**:233–253.

Sohn, R.A., S.C. Webb, J.A. Hildebrand, and B.C. Cornuelle. 1997. Three-dimensional tomographic velocity structure of upper crust, CoAxial segment, Juan de Fuca Ridge: Implications for on-axis evolution and hydrothermal circulation. *J. Geophys. Res.* **102**:17,679–17,695.

Solomon, S.C., and D.R. Toomey. 1992. The structure of mid-ocean ridges. *Ann. Rev. Earth Planet. Sci.* 2**0**:329–364.

Spudich, P., and J. Orcutt. 1980. A new look at the seismic velocity structure of the oceanic crust. *Rev. Geophys.* **18**:627–645.

Stein, C., and S. Stein. 1992. A model for the global variation in oceanic depth and heat flow with lithospheric age. *Nature* **359**:123–129.

Stein, C., and S. Stein. 1994. Constraints on hydrothermal heat flux through the oceanic lithosphere from global heat flow. *J. Geophys. Res.* **99**:3081–3095.

Stein, J.S., and A.T. Fisher. 2001. Multiple scales of hydrothermal circulation in Middle Valley, northern Juan de Fuca Ridge: Physical constraints and geologic models. *J. Geophys. Res.* **106**:8563–8580.

Toomey, D.R., S.C. Soloman, and G.M. Purdy. 1988. Microearthquakes beneath the median valley of the Mid-Atlantic Ridge near 23°N: Tomography and tectonics. *J. Geophys. Res.* **93**:9093–9112.

Tsang, C.F., and I. Neretnieks. 1998. Flow channeling in heterogeneous fractured rocks. *Rev. Geophys.* **36**:275–298.

Wilcock, W.S.D., S.D. Archer, and G.M. Purdy. 2003. Microearthquakes on the Endeavour segment of the Juan de Fuca Ridge. *J. Geophys. Res*., in press.

Wilcock, W.S.D., and J.R. Delaney. 1996. Mid-ocean ridge sulfide deposits: Evidence for heat extraction from magma chambers or cracking fronts. *Earth Planet. Sci. Lett.* **145**:49–64.

Wilson, D.S., D.A. Clague, N.H. Sleep, and J.L. Morton. 1988. Implications of magma chamber convection for the size and temperature of magma chambers at fast spreading ridges. *J. Geophys. Res.* **93**:11,974–11,984.